High-Efficiency Ripple-Free Power Converter for Nuclear Magnetic Resonance

J. Fernando Silva*¤, A. Galhardo*#, João Palma§#

* Centro de Automática da Universidade Técnica de Lisboa, Av. Rovisco Pais, 1, 1049-001, Lisboa, Portugal

¤ Department of Electrical and Computer Engineering, IST, SMEEP, Lisboa, Portugal

Departamento de Engenharia Electrotécnica e Automação, Instituto Superior de Engenharia de Lisboa, Portugal

§ Laboratório Nacional de Engenharia Civil, CPCE, Lisboa, Portugal

Abstract - A new power converter topology and control scheme, enabling a ripple free output with high efficiency, is presented. Feedback controllers for the proposed topology are designed taking into account non-ideal parameters. Experimental results, presenting almost no ripple, fast dynamics, almost no overshoot, and good tracking performance, demonstrate the merits and justify the cost of the extra amplifier needed in the new converter concept.

I. INTRODUCTION

The increasing demands of today power electronic apparatus, together with the rising quality requirements of applications like Nuclear Magnetic Resonance (NMR), which is a powerful analysis technique [1], or Digital Audio Power Amplifiers [2], [3], [4], [5], [6], can only be accomplished, if ripple free output waveforms are obtained together with the reduction of the equipment overall power consumption. In particular, fast field cycling NMR solenoids require current source power supplies, with adjustable output from a few ampere to hundreds of ampere, response times in the millisecond range and ripple content less than 10^{-3} of the desired current [1]. Switching power converters can easily supply the tens of ampere needed, with high efficiency, but to fulfil the prescribed ripple, non-realistic and interference prone switching frequencies should be used.

For ripple free outputs, linear power amplifiers could be used, at the cost of a degraded efficiency, since conventional linear power amplifiers have efficiencies usually lower than 25% [7]. Therefore, to increase the efficiency (reducing power consumption and enabling the use of small and lightweight power supplies and heat sinks, which minimise volume, weight and cost of equipment), switching Pulse Width Modulation (PWM) power converters should be used. However, too much ripple would be always present in the outputs. Consequently, new power converter topologies presenting efficiencies in the range 80%-90%, together with ripple free outputs, are desirable for the above mentioned applications.

This work is supported by FCT, Project PRAXIS/P/EEI/10235/98.

This paper presents a new paradigm to obtain ripple free PWM power converters. Using a parallel association of a sliding mode controlled PWM power converter with a conventional class AB linear amplifier [4], controlling the ripple free output variable, but supplying virtually zero output current, an overall high efficiency, ripple free, power converter is obtained. This topology is enhanced with a power supply equalising circuit. The PWM power converter supplies the needed power, while the class AB linear amplifier, acting as an active filter, supplies only the symmetric of the ripple component, therefore with much reduced power loss.

After presenting the new ripple free converter control concept (section II) and the modelling of the NMR dedicated converter, in section III, the paper considers the control issues in section IV. Section V demonstrates the usefulness of the new topology concept with experimental results, which show almost no ripple, fast dynamics, almost no overshoot, and good tracking performance.

II. NEW RIPPLE FREE POWER TOPOLOGY CONCEPT

Ripple free switching power converters can be obtained using a parallel association of a sliding mode controlled PWM power converter with a conventional class AB linear amplifier (Fig. 1). An inductor L is used to couple the PWM power converter to the output (voltage) of the class AB linear amplifier.

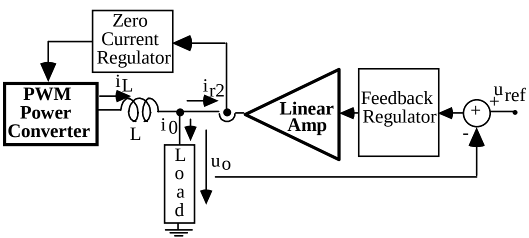

Fig. 1. New power converter topology with ripple free output waveform.

For NMR applications, as only two of the 3 currents (i_0, i_L and i_{r2}) are independent (Fig. 1), the control circuitry could be designed to enforce the PWM converter output current i_L mean value to follow the reference for the output current i_{0ref}

(Fig. 2). Then, the linear amplifier output current i_{r2} could be controlled to remove the i_L ripple (Fig. 2). Since $i_0 = i_L - i_{r2}$, ideally the output would be $i_0 = i_{0ref}$ (Fig. 2). However, small errors on i_L would introduce errors in i_0, since $i_{r2} \approx 0$. Another option, such as controlling i_L and i_0, could introduce even greater errors on i_{r2}, severely degrading the efficiency.

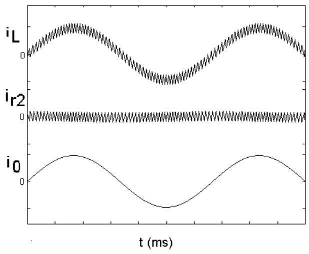

Fig. 2. Typical current waveforms of the power converter topology with ripple free output waveform (i_0).

Since a ripple free output is desired, the class AB linear amplifier should be controlled to enforce the ripple free desired output (i_0 or u_o) in the load (Fig. 1). Concurrently, as high efficiency is required, the linear amplifier output current must be almost zero. Therefore, the PWM power converter will be sliding mode controlled, to ensure that the output current of the class AB linear amplifier (i_{r2}) will be always contained within a hysterisis band, centred around zero, and with some tens of mA width.

This arrangement enables an overall high efficient power converter, since the PWM power converter supplies all the current i_L, which is approximately equal to i_0, since i_{r2} is close to zero. Therefore, almost no power is drawn from the class AB linear amplifier, and the ripple free output current i_0 (or the output voltage u_o) is guaranteed, by the linear amplifier plus feedback regulator, to follow the desired reference.

This topology concept will be applied to obtain a ripple free i_0 current source (Fig. 3), suitable for NMR systems. The circuit of Fig. 3 includes most effects that can influence the performance of the global system: parasitic resistors, low gain and bandwidth for the class AB linear amplifier, and inductive load. A sliding mode derived hysterisis controller drives the MOSFET transistors (Q1 and Q2) of the PWM power converter and a proportional integral (P.I.) linear regulator controls the output current i_0 (Fig. 3).

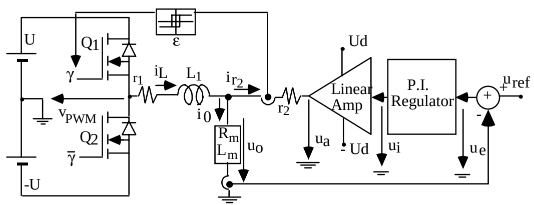

Fig. 3. PWM current source with zero ripple output.

III. SWITCHING CONVERTER & ACTIVE FILTER MODELLING

In the PWM power converter, neglecting switch delays, dead times, on state semiconductor voltage drops, snubber networks, power supply variations and supposing small dead times, the switching strategy must avoid internal shorts between the two switches of the half bridge leg, being the switches always in complementary states. The state of the switches can be represented by the time dependent switching variable $\gamma(t)$, defined as:

$$\gamma(t) = \begin{cases} 1 \longrightarrow \text{if Q1/D1 is ON and Q2/D2 is OFF} \\ -1 \longrightarrow \text{if Q1/D1 is OFF and Q2/D2 is ON} \end{cases} \qquad (1)$$

Therefore, the PWM power converter output voltage, v_{PWM}, can be written:

$$v_{PWM} = \gamma(t)\, U \qquad (2)$$

Considering the state variables and circuit components represented in Fig. 3, the switched state-space model (3) of the ripple free PWM converter can be obtained.

$$\begin{bmatrix} \dfrac{di_L}{dt} \\ \dfrac{di_0}{dt} \end{bmatrix} = \begin{bmatrix} -\dfrac{r_1+r_2}{L_1} & \dfrac{r_2}{L_1} \\ \dfrac{r_2}{L_m} & -\dfrac{R_m+r_2}{L_m} \end{bmatrix} \begin{bmatrix} i_L \\ i_0 \end{bmatrix} + \begin{bmatrix} \dfrac{\gamma(t)}{L_1} & -\dfrac{1}{L_1} \\ 0 & \dfrac{1}{L_m} \end{bmatrix} \begin{bmatrix} U \\ u_a \end{bmatrix} \qquad (3)$$

For this kind application, most class AB linear audio amplifiers present an input output transfer function including a gain A_d and a dominant pole at the frequency ω_p. Therefore:

$$\frac{u_a}{u_i} = \frac{A_d}{1+s/\omega_p} \qquad (4)$$

The proportional integral regulator, shown on Fig. 3, is represented by the following transfer function:

$$\frac{u_i}{u_e} = \frac{1+sT_z}{sT_p} = k_p + k_i/s \qquad (5)$$

The proportional and integral gains (respectively $k_p = T_z/T_p$ and $k_i = 1/T_p$) will be calculated in the next section, in order to achieve a current tracking behaviour. Hence, the linear amplifier maintains the i_0 current tightly controlled, extracting the ripple injected by the output current i_L of the PWM power converter. Only this extracted current ripple flows throughout the linear amplifier, dissipating very little power, often comparable with its quiescent power. In this type of operation, the linear amplifier performs as an active filtering device. Power supply U variations will be suppressed using an auxiliary converter leg discussed in section IV.

IV. CONTROLLING THE ZERO RIPPLE PWM CURRENT SOURCE

A. Sliding mode control of the switching converter to null the linear amplifier output current

To control the output current i_0 of this converter association, first the PWM power converter will be sliding mode controlled to maintain the current i_{r2} close to zero as much as possible. Using switching frequencies close to 100 kHz, the maximum current deviation from the zero value can be as low as 50-100mA, with the circuit values listed in section V. Analysing the circuit of Fig. 3 and using (3) the state space canonical form for the controlled current i_{r2} is:

$$\frac{d\, i_{r2}}{dt} = \frac{di_L}{dt} - \frac{di_0}{dt} = -\left(\frac{r_1+r_2}{L_1} + \frac{r_2}{L_m}\right) i_L + \left(\frac{r_2}{L_1} + \frac{R_m+r_2}{L_m}\right) i_0 + \frac{\gamma}{L_1} U - \left(\frac{1}{L_1} + \frac{1}{L_m}\right) u_a \tag{6}$$

From sliding mode control theory [8,9], a sliding surface, $S(i_{r2},t)$, ensuring robustness against supply and circuit parameter variations, is (since $i_{r2_{ref}}=0$):

$$S(i_{r2},t) = i_{r2_{ref}} - i_{r2} = -\, i_{r2} = 0 \tag{7}$$

From sliding mode stability [8,9] ($S(i_{r2},t)\,\dot{S}(i_{r2},t) < 0$) the switching strategy ensuring stability is:

$$\gamma(t) = -\,\mathrm{SGN}\left\{S(i_{r2},t) + \varepsilon\, \mathrm{SGN}\,[S(i_{r2},t\text{-}1)]\right\} \tag{8}$$

This switching law can be implemented using an hysterisis (2ε) comparator, as shown in Fig. 3.

B. Proportional Integral (PI) control of the linear power amplifier to obtain the desired load current

From (7), considering the robustness property of sliding mode, then $i_{r2} = 0$. This allows the second step on the design of the output current i_0 P.I. controller. The block diagram of the zero ripple PWM current source, obtained considering (3), (4), (5) and (7), is depicted in Fig. 4.

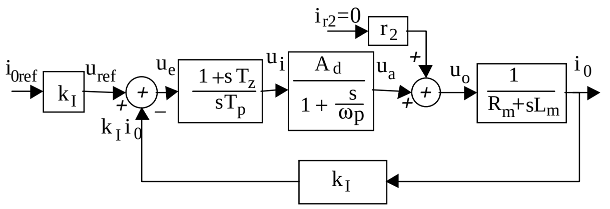

Fig. 4. Block diagram of the zero ripple PWM current source

To apply linear control theory to the block diagram of Fig. 4, consider:

$$\frac{i_0(s)}{u_o(s)} = \frac{1}{R_m + sL_m} \tag{9}$$

To achieve zero steady state error in i_0, which ensures steady state insensitivity to the perturbations, and to obtain closed loop second order dynamics, the PI controller (5) is selected. Cancelling the load pole ($-1/T_l$) with the PI zero ($-1/T_z$) yields:

$$T_z = L_m/R_m \tag{10}$$

The closed loop transfer function $i_0(s)/i_{0ref}(s)$, with zero perturbations, is:

$$\frac{i_0(s)}{i_{0ref}(s)} = \frac{\omega_p A_d k_I / (R_m T_p)}{s^2 + \omega_p s + \omega_p A_d k_I / (R_m T_p)} \tag{11}$$

The final value theorem enables the verification of the zero steady state error. Comparing the denominator of (11) to the second order polynomial $s^2+2\zeta\omega_n s+\omega_n^2$, yields:

$$\begin{aligned} \omega_n^2 &= \omega_p A_d k_I / (R_m T_p) \\ 2\zeta\omega_n &= \omega_p \end{aligned} \tag{12}$$

Since only one degree of freedom is left (T_p), the damping factor ζ is imposed. Usually $\zeta=\sqrt{2}/2$ is selected, since it often gives a fair compromise between response speed and overshoot. Therefore, from (12), (13) is derived:

$$T_p = 4\zeta^2 A_d k_I / (\omega_p R_m) = 2 A_d k_I / (\omega_p R_m) \tag{13}$$

Using (13) in (11) yields (14), the second order closed loop transfer function of the output current, showing that, with loads close to the nominal value, the dynamics depend only on the value $1/\omega_p$.

$$\frac{i_0(s)}{i_{0ref}(s)} = \frac{1}{2s^2/\omega_p^2 + 2s/\omega_p + 1} \tag{14}$$

Therefore, the dynamic characteristics of the linear amplifier determine the transient performance of the output current, imposing a response time of $2/\omega_p$, approximately:

$$\frac{i_0(s)}{i_{0ref}(s)} \approx \frac{1}{2s/\omega_p + 1} \tag{15}$$

To control the output current in order to achieve a steady state current tracking behaviour, the following proportional and integral gains can be obtained from (13) and (10).

$$k_p = \frac{L_m\ \omega_p}{2\ A_d\ k_I} \tag{16}$$

$$k_i = \frac{R_m\ \omega_p}{2\ A_d\ k_I} \tag{17}$$

C. Power supply capacitor voltage equalisation

Power supplies for NMR current sources often use diode rectifiers and filtering capacitors. As for fast field cycling NMR, the inductive load current i_0 is positive most of the time, capacitor C_2 (Fig. 5.b) charges (v_{02} increases) leading to unbalanced v_{01} and v_{02} voltages. Due to sliding mode robustness, the recovery of the load energy does not degrade the PWM converter performance. Nevertheless, the overvoltage can destroy the capacitor C_2. Therefore, to equalise v_{01} and v_{02}, the auxiliary reversible converter TR1, TR2, L_1, L_2, D1, D2, (Fig. 5.a) was conceived and simplified to obtain the equalising leg of the circuit of Fig. 5.b feeding L_E with current i_E.

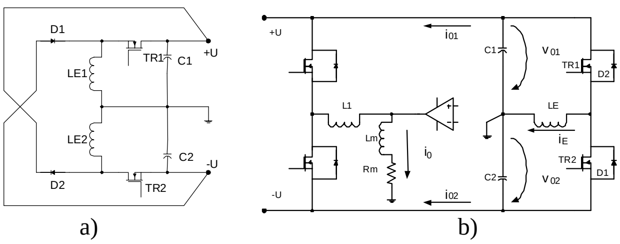

Fig. 5. a) Auxiliary reversible converter to equalise voltages of capacitors C_1 and C_2 ; b) Simplified circuitry of the overall zero ripple converter, showing the PWM leg (at left), linear amplifier, load and equalising leg (at right).

A switching function $\delta_1(t)$ is defined in order to analyse the auxiliary circuit of Fig. 5.b, ($\delta_1(t)$ =1, if TR1/D2 are ON and TR2/D1 are OFF; $\delta_1(t)$ =0, if TR1/D2 are OFF and TR2/D1 are ON). The switched state space model of the circuit is:

$$\begin{cases} L_E \dfrac{di_E}{dt} = \delta_1(t) v_{01} - (1-\delta_1(t)) v_{02} \\ C_1 \dfrac{dv_{01}}{dt} = -i_{01} - \delta_1(t) i_E \\ C_2 \dfrac{dv_{02}}{dt} = i_{02} + (1-\delta_1(t)) i_E \end{cases} \tag{18}$$

Subtracting the two last equations and supposing C_1=C_2=C, (19) is obtained.

$$\begin{cases} C\ \dfrac{dv_{01}}{dt} = -i_{01}(t) - \delta_1(t) i_E \\ \dfrac{d(v_{01}-v_{02})}{dt} = -\dfrac{i_{01}+i_{02}+i_E}{C} \end{cases} \tag{19}$$

To apply the sliding mode technique to the desired output v_{01}-v_{02}, which must satisfy (20), the time derivative of the last equation of (19) must be calculated, to express (21), the explicit dependence of v_{01}-v_{02} on the control variable $\delta_1(t)$.

$$(v_{01}-v_{02})_{ref} = 0 \tag{20}$$

$$\frac{d^2(v_{01}-v_{02})}{dt^2} = -\frac{1}{C}\left(\frac{di_{01}}{dt} + \frac{di_{02}}{dt} + \frac{\delta_1(t) v_{01}}{L_E} - \frac{(1-\delta_1(t)) v_{02}}{L_E}\right) \tag{21}$$

Since (21) implies a strong relative degree of two, and considering (20) the sliding surface $S(e_i,t)$ of (22) can be used, where k is related to the time constant of the v_{01}-v_{02} first order response.

$$\begin{aligned} S(e_i,t) &= \left[(v_{01}-v_{02})_{ref} - (v_{01}-v_{02})\right] + \\ &+ k\frac{d\left[(v_{01}-v_{02})_{ref} - (v_{01}-v_{02})\right]}{dt} = -(v_{01}-v_{02}) - k\frac{d(v_{01}-v_{02})}{dt} \end{aligned} \tag{22}$$

Using the first equation of (18) in (22), eq. 23 is derived.

$$S(e_i,t) = -\left[(v_{01}-v_{02}) - \frac{k}{C}(i_{01}+i_{02}+i_E)\right] \tag{23}$$

As i_{r2}≈0, then $i_{01} \approx i_0\ \gamma(t)$, $i_{02} \approx i_0\ (1-\gamma(t))$. Therefore, from (23):

$$S(e_i,t) = -\left[(v_{01}-v_{02}) - \frac{k}{C}(i_0+i_E)\right] \tag{24}$$

To ensure sliding mode stability, the condition $S(e_i,t)\,\dot{S}(e_i,t) < 0$ must be ensured. Therefore, from (25), the switching strategy for the control input $\delta_1(t)$ is expressed in (26) considering a comparator with hysterisis width $2\varepsilon_1$.

$$\dot{S}(e_i,t) = \frac{d(v_{02}-v_{01})}{dt} + \frac{k}{C}\frac{di_0}{dt} + \frac{k}{L_E C}(\delta_1(t) v_{01} - (1-\delta_1(t)) v_{02}) \tag{25}$$

$$\begin{cases} S(e_i,t) > \varepsilon_1 \Rightarrow \dot{S}(e_i,t) < 0 \Rightarrow \delta_1(t) = 0 \\ S(e_i,t) < -\varepsilon_1 \Rightarrow \dot{S}(e_i,t) > 0 \Rightarrow \delta_1(t) = 1 \end{cases} \tag{26}$$

The practical implementation (Fig. 6) of (24) and (26) gives, respectively, the controller and the modulator for the auxiliary converter. Notice that in steady state, with v_{01}-v_{02}=0, i_E = -i_0. Since the dynamics of $i_E(t)$ must be faster than the dynamics of $i_0(t)$, given the same supply voltages, $L_E < L_1 + L_m$ must be imposed.

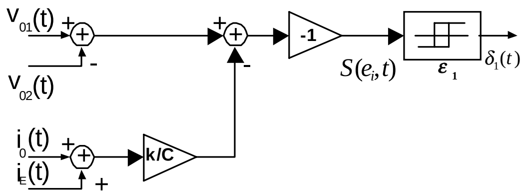

Fig. 6. Control hardware of the auxiliary equalising leg.

V. Results

A low power laboratory prototype was built with the following parameters: U≈50V, U_d≈30V, L_1≈1.4mH, R_m≈1.5Ω, L_m≈4mH, r_1≈0.1Ω, r_2≈0.05Ω. The linear amplifier LM1875 (A_d≈100, ω_p≈30krad/s) was used, driven by a PI with k_p=7 and k_i=2650s^{-1}. Gains and hysterisis widths (2ε≈0.2A) for the sliding mode controllers were adjusted to obtain switching frequencies near 100kHz for the PWM converter leg and 5kHz for the equalising leg.

The prototype of the near zero ripple PWM current source exhibits ripple free i_0 waveforms (Fig. 7.a, trace 4 and i_{0ref}, trace 1), fast dynamics (rise time nearly 0.3ms), almost no overshoot (≈1%, Fig. 7.a), negligible steady state errors (0.5%, Fig. 7.a) and good tracking performance (Fig. 9.a).

Notice that ripple (at nearly 100kHz) appears in the output current of the PWM power converter (i_L, Fig. 7.b trace 3) and in the input current of the linear amplifier (trace 2, -i_{r2}, Fig. 7.b), but not in the output current (i_0, Fig. 7.a) as the linear amplifier almost removes all the ripple content of the i_L current. This proves the usefulness of the proposed topology concept for supplying zero ripple waveforms.

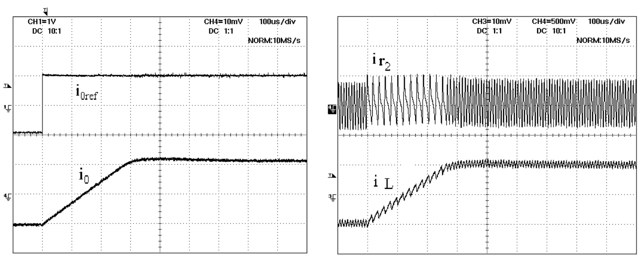

a) b)

Fig. **7.** Experimental results showing ripple free PWM current source step response (-1A to 1A); a) trace 1-the reference current i_{0ref} (1A/div), trace 4-the ripple free current i_0 (1A/div); b) trace 2-the ripple current i_{r2} extracted by the linear amplifier (0.1A/div), trace 3-the PWM converter output current i_L (1A/div).

Responses to current references typical of fast field cycling NMR are shown in Fig. 8 with a step from 1A to 3A. The response time is close to 0.3ms, as required, and there is no measurable overshoot or steady-state error. Fig. 9.a shows the limit of the tracking ability (sinusoidal reference with frequency 100Hz and 10A amplitude) and Fig. 9.b the slew-rate limited step response from 5A to 10A.

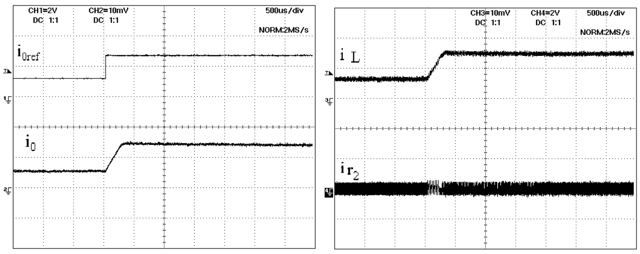

a) b)

Fig. 8. Experimental results showing typical fast field cycling current waveform (1A to 3A); a) trace 1-the reference current i_{0ref} (2A/div), trace 2-the ripple free current i_0 (2A/div); b) trace 3-the PWM converter output current i_L (2A/div), trace 4-the ripple current i_{r2} extracted by the linear amplifier (0.4A/div).

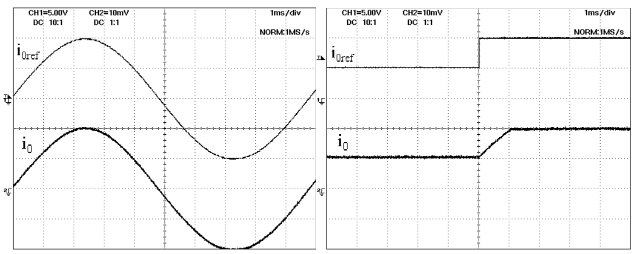

a) b)

Fig. 9. Experimental results showing dynamic behaviour a) tracking ability with sinusoidal reference, trace 1-the reference current i_{0ref} (5A/div), trace 2-the ripple free current i_0 (5A/div); b) 5A to 10A step response, trace 1-the reference current i_{0ref} (5A/div), trace 2-the ripple free current i_0 (5A/div).

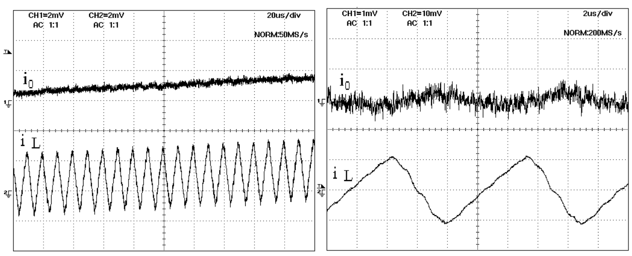

a) b)

Fig. 10. Residual ripple measurement; a) trace 1-the ripple free current i_0 (0.1A/div), trace 2- the PWM converter output current i_L (0.1A/div); b) trace 1-the ripple free current i_0 (10mA/div), trace 2- the PWM converter output current i_L (0.1A/div).

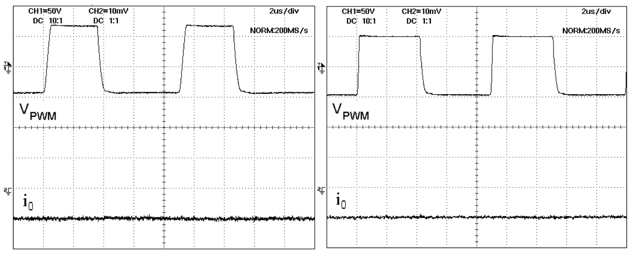

a) Without equalisation b) With equalisation

Fig. 11. Operation of the equalising converter leg at -1A output; a) Operation without equalisation, trace 1-the PWM converter output voltage v_{PWM} (50V/div) showing unbalanced positive (≈75V) and negative (≈45V) voltages, trace 2-the output current i_0 (1A/div); b) Operation with equalisation, trace 1-the PWM converter output voltage v_{PWM} (50V/div) showing balanced positive (≈50V) and negative (≈50V) voltages, trace 2-the output current i_0 (1A/div).

Fig. 10.a and 10.b show and allow the measurement of the residual ripple. From fig. 10.b the residual ripple (neglecting noise) is estimated to be 1mA, at 1A output current. The residual ripple figure is, therefore, close to 0.1%, which attest the very low ripple obtained. To obtain this low ripple using only a switching converter, a switching frequency near 10MHz would be necessary, implying higher switching losses and intolerable high electromagnetic interference in the NMR, since the proton frequencies are in this range.

Fig. 11.a shows the operation without power supply voltage equalisation. There is a strong unbalance between the positive supply (≈75V) and the negative voltage (≈-45V). Usually, this unbalance causes the power supply failure. Fig. 11.b shows the behaviour with the voltage equalisation leg operating. The positive and negative voltages are almost equal (≈50V). The visible small mismatches are due to practical errors and to the approximations made (C_1=C_2=C), which are not absolutely true in practice. This proves the usefulness of the equalising subsystem.

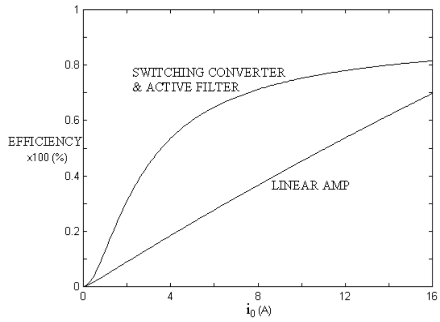

Fig. 12. Efficiency: comparison between the linear amplifier (supplying all the load current) and the proposed ripple free switching converter with active filter.

Efficiency of the proposed switching converter with active filtering is plotted in fig. 12. Compared to the efficiency of the linear amplifier supplying all the load current, the proposed converter always presents higher efficiencies. The linear converter efficiency increases with the load and peaks at the point of output transistor saturation. Even beyond this point the efficiency of the proposed converter would be higher since a higher voltage would be needed for the linear amplifier to maintain operation in the linear region.

VI. Conclusion

A new power converter topology concept, suitable for NMR power supplies, enabling ripple free outputs with high efficiency (≈80% at nominal load, with low supply voltages), was presented and one application example provided. Sliding mode and linear P.I. feedback controllers, respectively for the PWM power converter and equalising leg, and for the linear amplifier, were designed taking into account most non ideal parameters of the practical circuit. Obtained experimental results, showing almost no ripple (≈0.1%), fast dynamics, almost no overshoot, and good tracking performance, justify the extra cost of the needed linear amplifier and confirm the usefulness of the presented new topological/control concept.

References

[1] F. Noack, "NMR Field-Cycling Spectroscopy: Principles and Applications", Progress in NMR Spectroscopy, vol. 18, pp 171-276, 1986.

[2] S. Funada, H. Akya, "A study of high-efficiency audio power amplifiers using a voltage switching method", J. Audio Eng. Soc. Vol.32, no.10, Oct. 1984, pp 755-761.

[3] H. Nakagaki, N. Amada, S. Inoue, "A high-efficiency audio power amplifier", J. Audio Eng. Soc. Vol.31, no.6, June 1983, pp 430-436.

[4] R. A.R. Zee, A. J. M. Tuijl, "A high-efficiency low distortion audio power amplifier", 103rd Convention of the Audio Eng. Soc., reprint #4601, Sept 1997.

[5] B. E. Attwood, "Design parameters important for the optimization of very-high-fidelity PWM (class D) audio amplifiers", J. Audio Eng. Soc. Vol.31, no.11, Nov 1983, pp 842-853.

[6] M. B. Sandler, "Digital to analogue conversion using pulse width modulation", Electronics and Commun. Eng. Journal, Dec. 1993, pp.339-348.

[7] F. H. Raab, "Average efficiency of class-G power amplifiers", IEEE Trans on CE, Vol CE-32, no.2, May 1986, pp. 145-150.

[8] Utkin, V.; "Discontinuous Control Systems: State of Art in Theory and Applications", IFAC Proc, Munich, 7/1987, pp. 75-94.

[9] Hung, J.; Gao, W.; Hung, J., "Variable structure control": A Survey"; IEEE Transactions on Industrial Electronics, Vol. 40, nº. 1, pp. 2-22, February 1993.